EFDA–JET–PR(14)24

B. Cannas, A. Fanni, A. Murari, F. Pisano
and JET EFDA contributors

Nonlinear Dynamic Analysis of D_α Signals for Type I Edge Localized Modes Characterization on JET with a Carbon Wall

Nonlinear Dynamic Analysis of D_α Signals for Type I Edge Localized Modes Characterization on JET with a Carbon Wall

B. Cannas[1], A. Fanni[1], A. Murari[2], F. Pisano[1]
and JET EFDA contributors*

JET-EFDA, Culham Science Centre, OX14 3DB, Abingdon, UK

[1]Electrical and Electronic Engineering Department – University of Cagliari, Italy
[2]Consorzio RFX, EURATOM-ENEA Association, Italy
** See annex of F. Romanelli et al, "Overview of JET Results", (24th IAEA Fusion Energy Conference, San Diego, USA (2012)).*

Preprint of Paper to be submitted for publication in
Nuclear Fusion

ABSTRACT

Edge Localized Modes (ELMs) play a crucial role in present-day tokamak operation. Indeed, the Type-I ELMy H-mode has been chosen as the standard operation scenario for ITER. Thus, understanding and controlling ELMs are important issues for future machine design. In this paper, the dynamic characteristics of Type-I ELM time-series from the JET tokamak have been investigated. The dynamic analysis has been focused on the detection of nonlinear structure in Dα time series. The method of surrogate data has been applied to evaluate the statistical significance of the null hypothesis of static nonlinear distortion of an underlying Gaussian linear process. Several nonlinear statistics have been evaluated, such us the time delayed mutual information, the correlation dimension and the maximal Lyapunov exponent. The obtained results allow us to reject the null hypothesis, giving evidence of underlying nonlinear dynamics. Moreover, no evidence of low-dimensional chaos has been found; indeed, the analysed time series are better characterized by the power law sensitivity to initial conditions which can suggest noise contaminated quasi-periodic motion or the "edge of chaos" at the border between chaotic and non-chaotic dynamics.

1. INTRODUCTION

In large tokamaks the loss of a considerable amount of energy during an Edge Localized Mode (ELM) can cause damage to the first wall, especially in the divertor. On the other hand, the density of ELM-free H-mode plasmas is generally non-stationary and may uncontrollably rise until the plasma disrupts. Therefore, the cyclic degradation in confinement due to ELMs has a beneficial effect and allows stationary H-mode operations.

Understanding and controlling ELMs are crucial issues for the operation of ITER where the type-I ELMy H-mode has been chosen as the standard operation scenario [1].

A number of different ELM types were identified, and various models of ELMs were proposed [2, 3, 4, 5, 6, 7, 8], some of them, generated by the study of time series from different tokamaks, aimed at determining whether the ELM dynamics is deterministic or noise-dominated [9, 10, 11, 12, 13, 14, 15].

In [9], which is the first paper with this intent, the authors suggested that ELM occurrences exhibited a behaviour that is characteristic of the deterministic evolution of a low-order nonlinear dynamical system in a chaotic state. An important dynamical property, a period-one Unstable Periodic Orbit (UPO), was identified in one time series of inter-ELM intervals for JT60. The authors assessed the dimension of the ELM-time series at about 1.7 by evaluating the correlation sum. The correlation sum evaluation for surrogate data did not converge confirming the hypothesis of low-dimensional chaos for the analyzed shot.

In [10, 11] the authors applied a similar approach to 241 ELM-time series data from TCV. They considered the possibility that UPOs may occur by chance in a noise-dominated system and obtained results in disagreement with this hypothesis for a subset of discharges with $q_{95} > 2.6$. Moreover, in 100 discharges they observed frequent synchronization of the ELMs with sawteeth.

In contrasts with the findings in [10, 11], autoregressive moving average (ARMA) models were proposed in [12] to model the equations for 25 ELM time series measured in ASDEX Upgrade tokamak. The authors claimed that all detected deterministic components can be described by simple linear functions with input noise, which cannot generate complex chaos-like behavior.

The same data used in [10, 11] were re-examined in [13] where an improved surrogate generation method was applied to analyse the TCV inter-ELM time series against the null hypothesis that ELM dynamics is governed by an ARMA process. The null hypothesis was rejected adding confidence that chaotic dynamics are present in ELMs in TCV.

However, in [14, 15], the search for signature of chaos in ASDEX-Upgrade did not supply evidence of chaos. In particular, in [14] no UPOs were detected analysing 210 inter-ELM time series with the exception of five discharges. The authors ascribed the irregularity of the ELM time series to a noisy environment that affects the otherwise regular ELM cycle. In [15] the authors directly analysed 25 D_α time series, from shots with type I ELMs, to calculate dynamic invariants useful to detect chaos.

Surrogate time series obtained by shuffling original data were produced to provide a basis for comparison. As a result, no distinction between data and surrogates were discovered except for some time series.

Summarizing, due to the apparently aperiodic and unpredictable behaviour of ELMs, it is reasonable to investigate whether the ELM time series is predictable before trying to model the ELM cycle and forecast its development. An additional motivation of interest in this topic is related to the connection between the possibility of a chaotic behaviour and the issue of ELM control. In fact, chaotic systems can be controlled even without any knowledge of the system model, by exploiting its ergodic properties [16].

Given the results, sometimes conflicting, obtained in previous works, the aim of this paper is to investigate the dynamic characteristics of type I ELM nonlinear time series data from another machine, the JET tokamak, to try to confirm one of the proposed thesis, to understand the dynamic origin of ELM behaviour.

Data for this study are D_α time series grouped in cliques characterized by the same fixed experimental conditions and same distribution of inter-ELM time intervals [17].

Figure 1 shows the D_α time series for Pulse No: 74375 (I_p = 2.5MA, B_t = 2.5T, P_{NBI} = 15.1-15.5MW, δ_{LOW} = 0.33–0.35). As it can be seen, the time series exhibits early regular behavior (laminar flow) intermittently interrupted by outbreaks (bursts) at irregular intervals. Moreover, it increases more rapidly than it decreases, i.e., it is asymmetric. Thus, a first indication of nonlinearity can be obtained looking at the time series itself. However, all the bursts could come from a static strong nonlinearity, and all the serial correlations could be due to linear stochastic dynamics. The same could be stated for the asymmetry that does not imply a dynamic origin of nonlinearity.

Thus, in the present paper, the dynamic analysis has been firstly focused on the detection of eventual nonlinear structure in the time series. In order to test the presence of nonlinear dynamics

in the D_α time series, the method of surrogate data proposed in [18] has been applied. This is a more modest goal than the identification of chaos but it is crucial to prevent the misdiagnoses of deterministic chaos for noisy signals. A surrogate time series, obtained by static monotonic nonlinear transformation of a linear noisy process and a null hypothesis have been specified. The used surrogate time series has the same autocorrelation and the same amplitude distribution as D_α time series. Then, the distribution of quantities of interest for an ensemble of surrogate data sets, which are different realizations of the hypothesized linear stochastic process, has been determined.

Since a single reliable statistical test for nonlinearity is not available, combining multiple tests is a crucial aspect, especially when one is dealing with limited and noisy data sets as in this case. Moreover, particular care has been taken in choosing parameters and algorithms that, whilst helping to characterize the dynamics of the phenomenon, are robust with respect to the noise.

Moreover, the Time Delayed Mutual Information (TDMI), the Correlation dimension D_2 and the Maximal Lyapunov Exponent (MLE) have been evaluated to determine whether the observed irregular behaviour can be a consequence of deterministic chaotic dynamics [19]. In particular, non–integer correlation dimension and positive MLE indicate the possible presence of chaos. However, it is found [20] that similar results can be obtained even if data are not chaotic, for example in the case of linear or filtered white noise. Thus, if surrogate data analysis allows rejecting the null hypothesis, this is a good indication that data are dynamically nonlinear and possibly chaotic.

Moreover, to have a look at the high-dimensional phase space trajectory, the recurrence plot [21] has been created, which visualizes the recurrences of states in the phase space by a two-dimensional plot, locates hidden recurring patterns, non-stationarity and structural changes.

The paper is organised as follows: section II describes the database of D_α time series; section III describes the method of surrogate data; section IV presents the statistics chosen for detecting nonlinearity in the D_α time series; section V reports some comments on the effects of noise in the nonlinear analysis; section VI describes and discusses the obtained results. In Section VII the conclusions are drawn.

2. CASE STUDY CASE STUDY

In [17] a statistical analysis of 60 JET D_α signals, characteristic of JET Type-I ELMs with a carbon wall, was performed. The choice of the D_α signals was made by assuming that the ELM dynamics is perfectly observable from this measurement. To fulfil the stationarity requirements of the time series, the analysis was restricted to time intervals with fixed engineering conditions, in which the variations of plasma current (I_p), vacuum toroidal field at R = 2.96 (B_τ), total input power (P_{TOT}) and lower triangularity (δ_{low}) of the equilibrium field during the ELM phase have been considered. Only the experiments characterized by tolerances of ±4% for toroidal magnetic field, ±2% for plasma current, ±10% for total input power and lower triangularity, were taken into account. All tolerances were related to the signal resolutions. Only cases in which the heating power of the plasma has just only two contributions, ohmic power and neutral beam power (P_{NBI}), were considered.In addition,

all experiments dealing with ELM control and mitigation techniques were excluded.

The database consisted of 60 shots, corresponding to 24 experimental conditions with different values of I_p, B_τ, P_{NBI} and δ_{low} for a total of 3448 Type-I ELM time intervals.

After the localisation of the inter-ELM time intervals the memorylessness test suggested the presence of memory in the ELM time intervals for the considered Type-I ELMs, in agreement with previous studies [22].

From a statistical point of view, Type-I ELMs didn't show the same behaviour in their inter-ELM periods. Thus, the analysis were restricted to a homogeneous set of shots and pulses relative to similar inputs were grouped in 24 groups, including 10 singles, 4 pairs and 10 cliques. The groups are listed in Table I.

Kruskal-Wallis test [23] was applied to inter-ELM intervals of pulses of the same group to verify if they belong to the same population, i.e.,if they were groupable or not. Four groups (6, 10, 16, 19 in Table I) were identified with 5% confidence level, and the 19 shots belonging to those groups have been used for the dynamical analysis.

3. SURROGATE DATA

The interpretation of nonlinear measures can sometimes present problems since filtered noise time series can give rise to a spurious impression of low-dimensional dynamics and chaos. Thus, before applying nonlinear techniques to dynamic phenomena, the possible nonlinear nature of the data must be verified.

One of the most useful tools to take it into account is the use of surrogate data [18]. The surrogate data are generated in order to maintain the same linear properties, such as the power spectrum, the autocorrelation function and the probability distribution, as the original time series but destroying its nonlinear structure. The basic principle is straightforward: a nonlinear measure (dimension, entropy, etc.) is computed from a time series of interest and from a surrogate time series. If the outcome of the nonlinear analysis is clearly different for original and surrogate data, it can be concluded that the original data contain some interesting nonlinear structure. The comparison between original and surrogate data can be subjected to a formal statistical test by constructing not one but a whole set of surrogate data, and by determining whether the value of the nonlinear statistic for the original data lies within the distribution of values obtained for the ensemble of surrogate data.

Demonstration of nonlinearity is important since only nonlinear dynamical systems can have attractors other than a trivial point attractor and chaos can only occur in nonlinear dynamical systems. The generation of surrogate data is not foolproof. The use of amplitude-adjusted surrogate data [24, 25, 18] overcomes many pitfalls in the use of surrogate data, but caution is always appropriate. However, surrogate data provides the best check available against spurious detection of nonlinear dynamics.

With regards to the procedures, firstly a null hypothesis H0 is set, then a surrogate is created consistent with this null hypothesis. After this, if the measure evaluated on the surrogate series is

significantly different from that of the original time series, the null hypothesis is rejected.

The simplest null hypothesis which can be made is that the data $\{y_n , n = 0,...,N-1\}$ have been generated by some linear stochastic process with Gaussian increments

$$y_n = \sum_{i=1}^{n} a_i y_{n-i} + \sum_{i=0}^{n} b_i \eta_{n-i} \tag{1}$$

where $\{\eta_n\}$ are Gaussian uncorrelated random increments. This null hypothesis can also be formulated by stating that the only quantities of interest of the time series are the mean, the variance and the autocorrelation function. In this case, when the linear properties are specified by the squared amplitudes of the Discrete Fourier Transform (DFT)

$$Y_k = \sum_{n=0}^{N=1} y_n e^{-jn\frac{2\pi k}{N}} , \tag{2}$$

surrogate time series $\{y_n\}$ are readily created by multiplying the Fourier transform of the data by random phases and then transforming back to the time domain

$$\bar{y}_n = \frac{1}{N} \sum_{k=0}^{N=1} e^{j\alpha_k} |Y_k| e^{-jk\frac{2\pi n}{N}} , \tag{3}$$

where $0 \le \alpha_k < 2\pi$, respecting the symmetry condition $\alpha_{N-k} = \alpha_{-k} = -\alpha_k$, are uniform random numbers.

One disadvantage of this method is that it creates a surrogate time series with the same power spectrum, i.e. autocorrelation function, but having a distribution of values different from that of the original time series.

An alternative method which solves this problem is the so called Amplitude Adjusted Fourier Transform (AAFT), originally proposed by Theiler et al. [24]. This method is derived from a bit different null hypothesis, which takes into account the fact that usually the data do not follow a Gaussian distribution. This null hypothesis consists in the fact that the data $\{y_n\}$ have been generated by some linear stochastic process with Gaussian increments, distorted by a nonlinear static invertible function $f(.)$,

$$(x_n), \qquad x_n = \sum_{i=1}^{n} a_i x_{n=i} + \sum_{i=0}^{n} b_i \eta_{n-i} . \tag{4}$$

This kind of process is essentially linear since the only nonlinearity is contained in the measurement invertible function $f(.)$.

For the construction of the surrogate time series, the time series $\{y_n\}$ is rescaled to conform with a Gaussian distribution. The rescaling is made by simple rank ordering: an ordered random series with Gaussian distribution $\{g_n\}$ is created; let rank (y_n) be the position of the element y_n in $\{c_n\}$, which is an ordered copy of $\{y_n\}$, then the rescaled time series is given by $\{r_n = g_{\text{rank}(y_n)}\}$.

The rescaled time series $\{g_n\}$ is phase randomized using (3), conserving Gaussianity on average,

obtaining the new series $\{\bar{r}_n\}$. The resulting series $\{\bar{r}_n\}$ is rescaled to the empirical distribution of $\{y_n\}$, obtaining the new surrogate time series $\{\bar{y}_n = c_{rank(r_n)}\}$.

One disadvantage of this method is that it introduces a bias towards a slightly flatter spectrum [25] than that of the original time series. In [18] the authors propose a solution to this problem by the use of an iterative procedure. This procedure starts with a random shuffle without replacement or alternatively with an AAFT surrogate of the original time series $\{y_n\}$ obtaining the series $\{\bar{y}_n^0\}$. Then two steps are iterated until obtaining a surrogate whose probability distribution and power spectrum tend to those of the original series. The first step consists on taking the Fourier transform of $\{\bar{y}_n^{i-1}\}$, and replacing its squared amplitudes by those of $\{y_n\}$. During the second step the resulting series is rank ordered in order to assume exactly the same distribution of $\{y_n\}$.

In figure 2 a surrogate of D_α time series for Pulse No: 74375, created by using the algorithm proposed by Shreiber et al. [18], is shown.

Let Q denote a statistic computed for the original time series and $\bar{Q}_j$ the same statistics for the j-th surrogate generated under the null hypothesis H_0. Let $\bar{\mu}$ and $\bar{\sigma}$ denote the mean and standard deviation of the distribution of $\bar{Q}_j$. The significance is defined as [24]

$$\Sigma = \frac{|Q - \bar{\mu}|}{\bar{\sigma}}. \tag{5}$$

The rejection region for H0 is formed by a lower limit for Σ given from the critical value of the standard normal distribution at a pre-specified confidence level. If $\Sigma > 1.96$, H_0 is rejected at the 95% confidence level. It is worth noting that a lower value of $\bar{\sigma}$ results in a greater value of Σ, thus giving a high value of Σ even when Q is very close to $\bar{\mu}$. Moreover, the distribution of Σ is commonly non-Gaussian. For these reasons, the value of this parameter statistic should be interpreted with care.

An error bar on the estimation of Σ, based on error propagation theory, can be given by

$$\Delta\Sigma = \sqrt{\left(1 + \frac{1}{2}\Sigma^2\right)\frac{1}{N_\Sigma}}, \tag{6}$$

where N_Σ is the number of surrogates [24].

4. NONLINEAR ANALYSIS AND DISCRIMINATING STATISTICS

Any discriminating statistic can be employed in principle to investigate the possible nonlinear nature of a time series. In this paper, traditional nonlinear statistics have been chosen. In particular, since we are motivated by the question whether the underlying dynamics may be chaotic, the correlation dimension and the Maximum Lyapunov Exponent (MLE) have been evaluated. Moreover, to visualize the periodic nature of the trajectories through the highdimensional phase space, the structure of recurrence plots has been analysed.

4.1 LINEAR AND NONLINEAR CORRELATIONS

Autocorrelation refers to the correlation of a time series with its own past and future values.

Autocorrelation is also sometimes called “lagged correlation” or “serial correlation”, which refers to the correlation between members of a series of numbers arranged in time. A positive autocorrelation might be considered a specific form of “persistence”, a tendency for a system to remain in the same state from one observation to the next.

Autocorrelation measures the linear dependence of a variable with itself at two points at distance τ in the time series,

$$R_\tau = \frac{\sum_{n=0}^{N-1-\tau} y_n - \langle y \rangle_0^{N-1-\tau} \; y_{n+\tau} - \langle y \rangle_\tau^{N-1}}{\sqrt{\sum_{n=0}^{N-\tau-1} \left(y_n - \langle y \rangle_0^{N-1-\tau} \right)^2} \sqrt{\sum_{n=0}^{N-\tau-1} \left(y_{n+\tau} - \langle y \rangle_\tau^{N-1} \right)^2}} \tag{7}$$

where $\langle y \rangle_{n1}^{n2}$ represents the mean value of yn in the interval [n1, n2].

The mutual information is a measure of the amount of shared information gained on one system from the observation of another one. The average amount of information, that the variable contains about the variable itself delayed of a time lag Ω, is quantified by the time delayed mutual information (TDMI).

The TDMI is defined as:

$$I_\tau = \sum_{n=0}^{N-\tau-1} P\left(y_n, y_{n+\tau}\right) \log \left[\frac{P\left(y_n, y_{n+\tau}\right)}{P\left(y_n\right) P\left(y_{n+\tau}\right)} \right] \tag{8}$$

where $P(y_n)$ and $P(y_{n+\tau})$ are individual probabilities for the measurements of y_n and $y_{n+\tau}$. $P(y_n, y_{n+\tau})$ is the joint probability density for measurements y_n and $y_{n+\tau}$. For the evaluation of the probabilities, the time series is quantized using NB bins. The quantization can be made by using equal size bins or equal probability bins. Fraser et Al. [26] suggests the use of equal probability bins.

4.2 STATE SPACE RECONSTRUCTION

Let us consider a dynamical system

$$\frac{d\mathbf{x}(t)}{dt} = f(\mathbf{x}) . \tag{9}$$

The Takens embedding theorem states that the complete dynamics of a system can be reconstructed from a suitable time series n y , derived from the system taken at multiples of a fixed sampling time Δt [27]

$$y_n = y(\mathbf{x}(n\Delta t) . \tag{10}$$

Let us consider m–dimensional vectors

$$\mathbf{y}_n = [y_{n-(m-1)\tau^*}, y_{n-(m-2)\tau^*}, \ldots, y_{n-\tau^*}, y_n)] \tag{11}$$

whose components provide the coordinate system in which one can identify the attractor structure

associated with the observations. Then, there are two critical parameters involved in the construction of the delay coordinate embedding: the embedding dimension m and the time delay τ^*. Takens proved that, if $m \geq 2D + 1$, where D is the box counting dimension of the attractor, there exists a one to one correspondence between the state space reconstructed from the observation and the original state space. It is worth stressing that this is a sufficient but not necessary condition. In practice, an attractor may also be reconstructed successfully with the embedding dimension satisfying $m \geq D$.

The rational of the methods to evaluate the time delay τ^* is to choose the delay such that the coordinate components are only slightly correlated while still being close to one another.

A simple criterion was suggested in [28]. Let $R\tau$ be the autocorrelation function of the time series y_n. Theiler suggested selecting τ^* such that $R_{\tau^*} \cong e^{-1}$.

Fraser and Swinney [26] proposed a competing criterion based on the time delayed mutual information. This method defines how the measurements yn at time $n\Delta t$ are connected in an information theoretic fashion to measurements $y_{n+\tau}$ at time $(n + \tau)\Delta t$. The appropriate time delay τ^* is defined as the first minimum of the time delayed mutual information I_τ so that the values of yn and $y_{n+\tau}$ are independent enough of each other to be useful as coordinates in a time delay vector but no so independent as to have no connection with each other at all.

The embedding dimension m can be estimated through the method of False NearestNeighbors (FNNs) [29]. This method examines the fraction of nearest neighbours (NNs) as a function of m. The minimum m is found when most of the nearest neighbours do not move apart significantly in the next higher dimensional embedding.

Nonetheless, depending on the purpose of the embedding, there is less need to estimate m. For example, for the sake of dimension analysis or maximum Lyapunov exponent estimation, a criterion for accepting the estimate is the convergence of the estimate for increasing m, so that the analysis could rather be employed as a tool for determining the embedding dimension [30].

In some cases, the measured signal {yn} is quite uninteresting and the relevant information is contained in the time intervals between certain characteristic events. In thiscase, it could seem attractive to analyse the inter-spike intervals directly, but the embedding of these data in a standard way is questionable. Sauer [31] showed that, under quite general conditions, time intervals are phase space observables and therefore embedding theorems for the reconstruction of a state space from scalar signals are valid.

In case of $D\alpha$ time series, the time series of inter–ELM intervals result to be too short to allow the nonlinear analysis. Moreover, the relevant information contained in the time series behaviour would be lost, for example, in the case of events which are somewhere between spike or no spike. Thus, in this paper, the complete time series has been taken into account.

4.3 CORRELATION DIMENSION

The notion of correlation dimension was firstly introduced by Grassberger & Procaccia [32]. The idea behind this dimension's quantifier is that the weight of a typical ε-ball covering part of the

invariant set scales with its diameter like ε^D, where the value for D depends also on the way one defines the weight. The dimension used in this paper is called the correlation dimension D_2, and is computed by the correlation sum

$$C_{m,\varepsilon} = \frac{1}{N_{pairs}} \sum_{i=(m-1)\tau}^{N-2-w} \sum_{j>i+w} \Theta\left(\varepsilon - \left\|\mathbf{y}_i - \mathbf{y}_j\right\|\right) \tag{12}$$

where yn are m-dimensional delay vectors, $N_{pairs} = (N - w - (m - 1)\tau)(N - w - 1 - (m - 1)\tau)/2$ is the number of pairs of points covered by the sums, Θ is the Heaviside step function and w is the amplitude of the Theiler window, i.e., the time indices i and j must differ more than w is to exclude temporally correlated points from the pair counting. On sufficiently small length scales and when the embedding dimension m exceeds the box-dimension of the attractor,

$$C_{m,\varepsilon} = \propto \varepsilon^{D_2} \tag{13}$$

Since one does not know the box-dimension a priori, one checks for convergence of the estimated values of D_2 with m.

4.4 THE MAXIMUM LYAPUNOV EXPONENT

Lyapunov Exponents (LEs) quantify the exponential divergence of initially close state-space trajectories and estimate the amount of chaos in a system. The presence of a positive LE is important to represent local instability in a particular direction and helps in diagnosing chaos. Positive Lyapunov exponents, by themselves, do not always signify chaos. Indeed, the local instability can arise for a variety of reasons in different types of systems, e.g., noise itself. Supplementary information about the system is necessary to decisively identify chaos in a system.

No single universally accepted optimal method for computing the spectrum of LEs from time series data exists. Beyond inherent computational difficulties, one problem is given by the fact that reconstructed phase space has usually extra dimensions compared to the true phase space, leading to spurious LEs. Because estimating the maximum Lyapunov exponent is often of greatest interest in diagnosing chaos, many algorithms have been proposed to compute just the maximum Lyapunov exponent λmax. The most well-known of these algorithms are from Wolf et al. [33] and Sano and Savada [34].

Two alternative but more robust approaches were introduced by Kantz [35,19] and Rosenstein [36]. The issue of spurious exponents does not occur in the algorithms of Rosenstein and Kantz for computing λmax, which are robust to the choice of embedding dimension. Based on this understanding, the robust, consistent and unbiased estimator for the maximal Lyapunov exponent proposed by Rosenstein and implemented in the TISEAN time series analysis package [37] has been used in this paper.

4.5 RECURRENCE PLOTS

The Recurrence Plots (RPs) are modern methods of nonlinear data analysis. The tool for RPs, introduced in 1987 by Eckmann et al. [21], allows the visualization of a square matrix, in which the matrix elements correspond to those times at which a state of a dynamical system recurs revealing if the phase space trajectory visits roughly the same area. The advantage of RPs is that they can also be applied to rather short and even non-stationary data.

Since usually the phase space does not have a dimension (two or three) which allows it to be pictured, the m-dimensional phase space is reconstructed from the time series to be analyzed.

The RP can be mathematically expressed by a two-dimensional squared matrix, the so called recurrence matrix

$$\mathcal{R}_{i,j} = \Theta\left(\varepsilon^* - \left\|\mathbf{y}_i - \mathbf{y}_j\right\|\right), \quad \mathbf{y}_i, \mathbf{y}_j \in \mathbb{R}^m, \quad i, j = 0, \ldots, N-1 \tag{14}$$

where ε* is a threshold distance. Each element of the recurrence matrix represents the recurrence of a state at time i at a different time j, equal to one if the distance between the two states is lower than ε, and equal to zero otherwise. By plotting the recurrence matrix in a square map where both axes are time axes and assigning black dots to ones and white dots to zeroes, it is possible to obtain the recurrence plot.

Since $\mathcal{R}_{i-j}, \forall_i$ by definition, the RP has always a black main diagonal line, the line of identity (LOI). Furthermore, the RP is symmetric by definition with respect to the main diagonal, ($\mathcal{R}_{i-j} = \mathcal{R}_{j-i}$).

In literature several variations of the recurrence plots have been proposed. Iwanski and Bradley [38] proposed to plot directly the distance matrix

$$\mathcal{D}_{i,j} = \left\|\mathbf{y}_i - \mathbf{y}_j\right\|, \quad \mathbf{y}_i, \mathbf{y}_j \in \mathbb{R}^m, \quad i, j = 0, \ldots, N-1, \tag{15}$$

instead of the recurrence matrix. Although this is not an RP, it is sometimes called unthresholded recurrence plot (UTRP). By using an appropriate colour bar it is possible to highlight the different recurrence structures at different thresholds.

Iwanski and Bradley [38] found that the appearance of recurrence plots for certain low-dimensional systems are not significantly altered by a small change in the embedding dimension, suggesting that these plots may supply important new invariant characteristics of a system.

5. ANALYZING NOISY SIGNALS

Mathematically speaking, the presence of noise poses some problems to the estimation of the nonlinearity measures. It is worth noting that Takens theorem assumes that the observable signal is noiseless. Nevertheless, in the practice, in almost every experimental system, data include some level of stochastic noise, whether intrinsic or external with respect to the examined system. Sometimes the presence of noise alters the percentage of false neighbours in the FNN algorithm and the estimation

of the correlation dimension, since the correlation dimension does not converge with the increase of the embedding dimension. Therefore, in the case of noisy systems, it is better to be cautious in drawing conclusions about the actual size of the attractor. It is worth noting that a number of samples $N < 10^{D/2}$, where D is the estimated correlation dimension, doesn't allow to differentiate noise from finite-dimensional deterministic data, and thus the estimated D becomes unuseful [39]. Also findings of positive Lyapunov exponents, by themselves, should never be taken as conclusive proof of chaos without substantial additional evidence that supports the deterministic origin of the sensitive dependence on initial conditions that the Lyapunov exponents quantify. Franca and Savi [40] found that the Sano and Sawada [34] and Wolf et al. [33] algorithms are especially sensitive to measurement noise, whereas the algorithms from Rosenstein and Kantz are not. The algorithms proposed by Rosenstein and Kantz describe the underlying nature of the divergence, exponential or otherwise, and thus allow one to extract quantifiable statistics related to the dynamics of the system being studied. Regardless of whether these statistical quantities constitute true "Lyapunov exponents", they can still provide valuable insights into the underlying dynamics by characterizing the inherent sensitivity of the system to small perturbations. Such insights may be far more valuable to the understanding of mechanisms responsible for those dynamics than any arbitrary distinction between "chaotic" or "not chaotic" [41].

With regard to the influence of noise on LEs evaluation, Tsallis et al. [42] generalized the concept of ESIC (Exponential Sensitivity to Initial Conditions) to PSIC (Power Law Sensitivity to Initial Conditions), to characterize the dynamical behavior typical of a type of motion whose complexity is neither regular nor fully chaotic or random. This behavior can be found especially in noisy systems at the edge of chaos, i.e., noisy chaotic systems with a maximum positive Lyapunov exponent close to zero. These systems are characterized by power law sensitivity to initial conditions, instead of the exponential sensitivity, and are considered as weak chaotic systems. Weak chaotic systems exhibit anomalous dynamics characterized by the non-equivalence of time and ensemble averages, the so called weak ergodicity breaking [43]. Low-dimensional nonlinear maps are prototype models to study this typical behavior [44].

In [45] the consequences of noise on different maps at the edge of chaos have been investigated: noise-free logistic and Henon maps at the edge of chaos do not evidence PSIC. However, motions around the edge of chaos, being they simply regular or truly chaotic, all collapse, in the presence of dynamic noise, onto the PSIC attractor. Hence, dynamic noise makes PSIC observable.

Principal Component Analysis

Since linear or at least smooth transformations of the delay vectors do not change the validity of the embedding theorems, some particular manipulations of the delay vectors may be useful for a better representation of the data, especially in the case of noisy measurements, in which an implicit reduction of the noise is often required. Principal component analysis (PCA) [46], also known as Karhunen–Loeve Transformation or Singular Value Decomposition, is a tool which can be used for this purpose. PCA was proposed by [47] as a coordinate transformation method for a delay

embedding space of a single experimental measurement. The benefits of projecting delay coordinates on principal component basis, particularly in the case of noisy data, were extensively studied also by [48, 49, 50]). The main idea is to characterise the time series by its most relevant components in a delay embedding space of dimension m probably larger than strictly necessary.

Algorithmically, the principal components are evaluated by computation of the covariance matrix. Since the covariance matrix is real and symmetric, it presents real eigenvalues and orthogonal eigenvectors. The q most relevant directions in space, which contain most of the variation present in the data, are thus given by the eigenvectors corresponding to the largest q eigenvalues. In the case of isotropically distributed noise, since the first q principal components have maximum variance of the data, they have also the maximum signal to noise ratio (SNR). Thus, the use of a high dimension m and the projection onto the first q principal components generally acts like noise filtering [51,35, 37] proposed to choose a much shorter delay, than one would use for an ordinary time delay embedding, while at the same time increasing the embedding dimension, in order to take advantage of the noise averaging effect.

6. RESULTS RESULTS

Autocorrelation and Mutual information Figure 3(a) shows the autocorrelation function R_τ of the D_α time series and its surrogates for Pulse No: 74375. As it can be noticed, there is a substantial agreement between D_α time series and surrogate data, confirming that surrogate data preserve the linear properties of the original data.

Figure 3(b) and 3(c) show the time delayed mutual information I_τ of the D_α time series for Pulse No: 74375, with 16 equal size bins and equal probability bins, respectively. The TDMI evaluated with equal size bins attains values close to zero for time lags greater than 50, indicating that a time series delayed with a time lag greater than 50 is almost independent by the original non-delayed time series, losing all nonlinear correlations.

At short lags there is a clear difference between D_α time series and surrogate data; original data give larger TDMI for a longer range of lags ($\tau \leq 25$). As shown in Fig. 3(d) the significance Σ of the TDMI with its error bar attains values approximately $(5 - 20)\cdot\sigma$ for $\tau \leq 25$, thus rejecting the null hypothesis with very high confidence level.

The TDMI evaluated with equal probability bins decreases rapidly for $\tau = 1$ and keeps on decreasing more slowly for greater values of τ. There is a clear difference between $D\alpha$ time series and surrogate data also for greater values of τ. In Fig. 3(e) the significance Σ with its error bar is shown, highlighting this difference.

Figure 4 shows the same quantities for Pulse No: 76428 ($I_p = 2MA$, $B_t = 2T$, $P_{NBI} = 7.5MW$, $\delta_{LOW} = 0.35$), characterized by a slower mean frequency than the one of Pulse No: 74375. As it can be noticed, there is a minimum in both the autocorrelation function and the time delayed mutual information with equal size bins at $\tau \cong 50$. In this case, TDMI of original and surrogate data differs also for higher lags, showing a significant difference between original data and surrogates. Since

similar results has been found for all the time series of the database, this indicates the non-random and nonlinear character of the D_α time series.

6.1. TIME DELAY EMBEDDING

Regarding the evaluation of the time delay, for the majority of shots, I_τ does not exhibit a distinct minimum, and we have to look for some alternative criterion such as, e.g., the first delay, where a steep decay of the TDMI changes to a slow decay or a plateau. For example, for Pulse No: 74375, if we examine TDMI with equal size bins we can assume that a suitable τ may be chosen in the interval of the fast descent of I_τ, i.e., $0 < \tau < 25$. Conversely, the TDMI with equal probability bins shows a fast descent for $0 < \tau < 1$.

Also the autocorrelation function may be applied to help in the determination of a reasonable delay. For Pulse No: 74375, the autocorrelation drops below e^{-1} for $\tau = 11$. To support the choice of τ^*, the shape of obtained orbits in 3D projection for $\tau^* = 11$ (figure 5(a)) and $\tau^* = 1$ (figure 5(b)) has been considered. As it can be noticed, by using $\tau^* = 11$, the first three components of the attractor remain almost independent (even worse for $\tau^* = 25$). If we consider that the rise time of a burst is about 2-3 sampling times, it can be assumed that a smaller τ^* is necessary. In figure 5(b) it is clear that, with $\tau^* = 1$, the attractor is smoother and better unfolded. This choice is supported by the results on the TDMI with equal probability bins. This short lag allows a delay reconstruction with a central hole (for pseudo-periodic dynamics such this may be, it is reasonable to presume that the central region will exhibit an unstable focus). Thus, the chosen value is $\tau^* = 1$. The same conclusion can be reached by analysing the other time series.

The second parameter to be chosen , required for the reconstruction of the embedding space, is the embedding dimension. To determine the appropriate embedding dimension, the False Nearest Neighbours method has been used. Figure 6 shows the results of the estimations of the embedding dimension for Pulse No: 74375.

The estimated embedding dimension could be evaluated as the shortest m for which the percentage of false nearest neighbours is lower than 30%. For Pulse No: 74375, the estimated embedding dimension is m = 5, as indicated by the red square in Figure 6. It is worth noting that this estimation might be greater than the right embedding dimension due to the presence of noise in the signal.

The obtained values for m in all the considered shots belong to the range m = 4 – 7 and are shown in Table II.

For a better visualization of the dynamics of the attractor and to filter the noise component of the signal, it is advisable to use some filtering strategy, as the principal component analysis. In order to take advantage of the noise averaging effect of the principal component scheme, it is worthwhile to increase the embedding dimension while using a short time delay (for this purpose □ = 1 is a good choice). Hegger [37] suggests the use of an embedding dimension for PCA equal or larger than twice the estimated m.

For Pulse No: 74375, an embedding dimension m = 10 has been used for PCA projection.

Figure 7(a) and (b) show the projections on the plane described by the first and second principal components and by the second and third components respectively. Similar forms can be seen for the other shots. As it can be noticed, PCA supplies a better representation of the attractor, which highlights the ELM cycle main dynamics. Figure 7(c) shows the scree plot, which graphs the variance, normalized with respect to the total variance, described by each principal component. Figure 7(d) shows the cumulative variance described by the principal components. The first three principal components supply more than 88% of the total variance. It is worth noting that the signal tolerance on the measurement is about 20%.

6.2. CORRELATION DIMENSION

Figure 8(a) and (b) respectively show the correlation integral $C_{m,\varepsilon}$ as a function of ln(ε) and the correlation dimension D2 as a function of m for the D_α and surrogate time series, using $\tau^* = 1$, m = 1–9, Theiler parameter $w = 3 \cdot \tau^* = 3$, for Pulse No: 74375. Figure 8(c) shows the value of significance Σ of the correlation dimension D_2 with its error bar for m = 5. The slopes do not reveal efficient scaling and low saturation values. The usual cause of this lack of convergence is the presence of a relatively high-dimensional attractor and a small data set. Large levels of noise have a similar effect because the noise fills out the attractor at small enough scales.

Furthermore, the analysis with surrogate data shows evidence of nonlinearity. We are able to reject the null hypothesis that data arise from monotonic nonlinear transformation of a linear stochastic Gaussian process, thus we can assess that the system underlying the process under study is nonlinear.

Although the correlation dimension does not saturate with m it attains small values. Thus, by taking into account the information obtained both by PCA and surrogate data, we can assume that the system underlying the process under study is low dimensional and nonlinear.The same result can be obtained for the other shots.

6.3. MAXIMUM LYAPUNOV EXPONENT

In figure 9, different plots of the mean logarithm of the divergence of initially close trajectories, evaluated with Rosenstein algorithm for Pulse No: 74375, are shown. In particular, figure 9(a) shows the behavior of the mean logarithm of divergence for original time series and for different values of m (in red that related to m = 5, result of the FNN algorithm, and in blue those related to the other values of $m \leq 9$). As it can be noticed, the behavior is similar for all $m \geq 3$ suggesting the hypothesis that the real embedding dimension of the attractor is equal to m = 3.

In Figure 9(b) and (c) the curves for the original time series and for surrogates for $m > 5$ have been vertically translated close to those for m = 5 for the sake of slope visualization. As it can be noticed, the behavior of the curves of the original time series is widely different than the ones of the surrogates. Figure 9(c) shows a zoom of the same curves in the first time instants , which highlights the lack of a linear increasing of the curves, i.e., a lack of exponential divergence. Note that in these

cases the values of the ln<divergence> are meaningless.

By using a logarithmic scale in the time axis (Fig.9(d)), it is possible to identify a power law sensitivity to initial conditions (PSIC), more or less between 1 and 10ms, as indicated by the black fitting line. This suggests the hypothesis of a low-dimensional noisy weak-chaotic system.
A similar behaviour has been found for the other shots.

6.4 RECURRENCE PLOTS

Fortunately, the recurrence plot is not particularly sensitive to the choice of embedding parameters and we found only marginal, almost invisible differences when choosing embedding dimension and time delay within reasonable ranges.

In Fig.10 typical UTRP is shown (Pulse No: 74375). As it can be noticed, white corridors are present when ELMs appear. Dark squares or rectangular blocks among white corridors correspond to laminar phases. The points which lie along and close to the diagonal blocks are darker than the others and correspond to the similarity between laminar phases.

As shown in Fig.11, by introducing the threshold $\varepsilon^* = 0.1$, the RP is characterized by squares and rectangles with an elongated lower left corner. The shape resembles a uniformly black kite-like.

The RPs in Fig.11 are very similar to those reported in [52] for coupled nonlinear maps (see Fig.12), models of type-II intermittency. All plots exhibit the same characteristic kite-like shape, despite the different orientation.

From a mathematical point of view type II intermittency is due to a subcritical Hopf bifurcation: two complex conjugate eigenvalues of the map exit the unit circle away from the real axis. Pomeau and Manneville conjectured that there must exist a global nonlinear mechanism that reinjects the trajectory in the vicinity of the focus. To simulate this nonlinear behavior, they consider the trajectory randomly reinjected around the focus. However, they do not specify this global nonlinear bifurcation scenario.

The laminar phase occurs when the trajectory of the system is injected close to that unstable fixed point. The trajectory then forms a spiral outward from the fixed point. When the trajectory leaves this region the chaotic phase occurs ending with the reinjection.
This similarity suggests further investigation of intermittent systems with the aim of fitting experimental data and modelling Type-I ELMs.

CONCLUSIONS

The dynamic origin of the apparently random variations in Type-I ELMy H-mode time series has been addressed. Several nonlinear dynamical indicators have been evaluated for some $D\alpha$ time series recorded in the JET database with a carbon wall. The methods used for the nonlinear dynamic analysis have been strongly limited by typical features of experimental situations. In particular, the presence of broadband noise presents severe difficulties for correlation dimension algorithms, and our attempts to extrapolate a reliable estimate of the correlation dimension failed. Also the strong

intermittency in the time series poses a practical problem, in that it implies a large time scale over which the signal does not look stationary.

Although the obtained results do not prove that ELM time series are definitely chaotic, they are found to be consistent with the hypothesis of noisy weak-chaotic dynamics.

The hint that nonlinear behavior plays a role comes from the data itself: the signal is not compatible with the assumption that it is created by a Gaussian random process with only linear correlations, possibly distorted by a nonlinear measurement function. This is shown by creating an artificial surrogate data set which has exactly the same linear properties but has no further determinism built in. This data set consists of random numbers which have been rescaled to the distribution of the values of the original, and filtered so that the power spectrum, and so the autocorrelation function, is the same. If the measured data are properly described by a linear process eventually distorted by a static nonlinearity we should not find any significant differences from the artificial ones.

The analysis of the results obtained with time delayed mutual information, principal components analysis, correlation dimension, maximum Lyapunov exponent and recurrence plots suggests the noisy and nonlinear character of the time series.

Regarding the mutual information there is a clear discrimination between $D\alpha$ time series and surrogate data, either with equal size or equal probability bins; original data give larger time delayed mutual information for a longer range of lags and the null hypothesis can be rejected with very high confidence level.

A graphical analysis of the attractor joined to an analysis of the time delayed mutual information and of the autocorrelation function has suggested the use of a small time delay $\tau^* = 1$. With regards to embedding dimension m, the FNNs algorithm shows that the percentage of FNNs falls off under 30% when the dimension is greater than four.

Moreover, the attractor obtained with the first three PCs appears quite well unfolded.

The correlation dimension and the MLE have been evaluated for a wide range of values of m. The test on the correlation dimension is very sensitive to noise, which is present in the data, and hence rarely provides definitive answers. However, the analysis with surrogate data shows evidence of nonlinearity, in fact we are able to reject the null hypothesis that data arise from monotonic nonlinear transformation of a linear stochastic Gaussian process. Since the correlation dimension attains small values we expect that the system is low dimensional. The fact that the correlation dimension does not saturate with m is attributed to the effects of noise. The calculation of the maximum Lyapunov exponent does not show exponential divergence of trajectories but power law sensitivity to initial conditions which can suggest noisy quasi-periodic motion or a motion at the "edge of chaos", at the border between chaotic and non-chaotic dynamics. This is a type of dynamics that is intermediate between strongly chaotic, in the sense of exponential sensitivity quantified by a positive Lyapunov exponent, and trivially being non-chaotic in terms of purely regular dynamics. With regards to the role of the noise, the dynamic noise seems of crucial importance for the observation of PSIC. For example, by studying noise-free and noisy logistic and Henon maps near the edge of chaos, Gao [45]

found that when there is no noise, the PSIC attractor cannot be observed from a scalar time series. However, when dynamic noise is present, motions around the edge of chaos collapse onto the PSIC. The qualitative analysis of RPs adds further confidence to this interpretation of the phenomena, revealing typical kite-like shapes, that can be found in low-dimensional nonlinear maps modeling intermittent phenomena.

Such kind of maps have been introduced by Pomeau and Manneville to describe the intermittency routes to chaos. In particular, in type II intermittency, the most unknown transition to chaos, a fixed point of the system becomes a repelling focus when two conjugate complex eigenvalues cross the unit circle and causes the spiraling behavior. It is worth noting that the Pomeau-Manneville maps are prototype models to study the behavior of systems exhibiting weak chaos. It is possible to generate power-laws from simple iterative maps by fine-tuning the parameters of the system at the edge of chaos where the sensitivity to initial conditions of the map is a lot milder than in the chaotic regime. Summarizing, in the past three decades, a lot of papers on time series analysis and specifically on ELM analysis have been published under the framework of the standard chaos theory. However, there is a marked lack of a unified interpretation of the phenomenon. Chaotic dynamics in the rigorous mathematical sense is seldom observed, probably due to the ubiquity of noise in experimental time series. Also in case of Dα time series we cannot assert that the signals are chaotic in the rigorous mathematical sense but a weak chaos regime could be identified. This is the main reason that the phenomenon is better characterized by the power law sensitivity to initial conditions instead of the exponential sensitivity to initial conditions framework.

As a first stage of the characterization process, interpreting ELM time series from the standpoint of PSIC and intermittency is a fundamental information to approach at the choice of a proper dynamical model, which will be the subject of future investigations. In this direction, low-dimensional nonlinear maps appears to play an important role in the ELM model development.

ACKNOWLEDGMENTS

This work was supported by EURATOM and carried out within the framework of the European Fusion Development Agreement. The views and opinions expressed herein do not necessarily reflect those of the European Commission.

REFERENCES

[1]. D.C. McDonald, Y. Andrew, G.T.A. Huysmans, A. Loarte, J. Ongena, J. Rapp, S. Saarelma (2008), “Chapter 3: ELMy H-mode operation in JET”, Fusion Science and Technology, vol. **53** (4), pp.891–957.

[2]. J. -N. Leboeuf, L.A. Charlton, B.A. Carreras (1993), “Shear flow effects on the nonlinear evolution of thermal instabilities”, Physics of Fluids B: Plasma Physics, vol. **5** (8), pp. 2959–2966.

[3]. O. Pogutse, W. Kerner, V. Gribkov, S. Bazdenkov, M. Osipenko (1994), “The resistive

interchange convection in the edge of tokamak plasmas", Plasma Physics and Controlled Fusion, vol. **36** (12), pp. 1963–1985.

[4]. V.B. Lebedev, P. H. Diamond, I. Gruzinova, B.A. Carreras (1995), "A minimal dynamical model of edge localized mode phenomena", Physics of Plasmas, vol. 2 (9), pp. 3345–3359.

[5]. W. Horton, G. Hu, G. Laval (1996), "Turbulent transport in mixed states of convective cells and sheared flows", Physics of Plasmas, vol. **3** (8), pp. 2912–2923.

[6]. J.W. Connor (1998), "Edge-localized mode – Physics and theory", Plasma Physics and Controlled Fusion, vol. **40** (5), pp. 531–542.

[7]. G.T.A. Huysmans, S. Pamela, E. Van Der Plas, P. Ramet (2009), "Non-linear MHD simulations of edge localized modes (ELMs)", Plasma Physics and Controlled Fusion, vol. **51** (12), p. 124012.

[8]. W. Arter (2009), "Symmetry constraints on the dynamics of magnetically confined plasma", Physical Review Letters, vol. 102 (19), p. 195004.

[9]. P.E. Bak, R. Yoshino, N. Asakura, T. Nakano (1999), "Identification of Unstable Periodic Orbit in Inter–Edge-Localized-Mode Intervals in JT-60U", Physical Review Letters, Vol. **83** (7), pp. 1339–1342.

[10]. A.W. Degeling, Y.R. Martin, P.E. Bak, J.B. Lister, X. Llobet (2001), "Dynamics of edge localized modes in the TCV tokamak", Plasma Physics and Controlled Fusion, vol. **43** (12), pp. 1671–1698.

[11]. Y. R. Martin, A.W. Degeling, J. B. Lister (2002), "Search for determinism in ELM time series in TCV", Plasma Physics and Controlled Fusion, vol. **44** (5A), pp. A373–A382.

[12]. G. Zvejnieks, V. N. Kuzovkov, O. Dumbrajs, A. W. Degeling, W. Suttrop, H. Urano, H. Zohm (2004), "Autoregressive moving average model for analyzing edge localized mode time series on Axially Symmetric Divertor Experiment (ASDEX) Upgrade tokamak", Physics of Plasmas, vol. **11** (12), pp. 5658–5667.

[13]. A.W. Degeling, J. B. Lister, Y. R. Martin, G. Zvejnieks (2004), "Were the chaotic ELMs in TCV the result of an ARMA process?", Plasma Physics and Controlled Fusion, vol. **46** (10), pp. L15–L21.

[14]. V. Hynonen, O. Dumbrajs, A.W. Degeling, T. Kurki-Suonio, H. Urano (2004), "The search for chaotic edge localized modes in ASDEX Upgrade", Plasma Physics and Controlled Fusion, vol. **46** (9), pp. 1409–1422.

[15]. M.J. Ikonen, O. Dumbrajas (2005), "Search for Deterministic Chaos in ELM Time Series of Asdex Upgrade Tokamak", IEEE Transaction on Plasma Science, vol. **33** (3), pp. 1115–1122.

[16]. S. Boccaletti, C. Grebogi, Y. –C. Lai, H. Mancini, Maza (2000), "The control of chaos: theory and applications", Physics Reports, **329** (3), pp. 103–197.

[17]. A. Murari, F. Pisano, J. Vega, B. Cannas, A. Fanni, S. Gonzales, Gelfusa, M. Grosso (2014), "Extensive Statistical Analysis of ELMs on JET with a Carbon Wall", Plasma Physics and Controlled Fusion. (accepted with minor revisions)

[18]. T. Schreiber, A. Schmitz (1999), "Surrogate time series", Physica D: Nonlinear Phenomena, vol. **142** (3–4), pp. 346–382.

[19]. H. Kantz (1994), "A robust method to estimate the maximal Lyapunov exponent of a time series", Physics Letters A, vol. **185** (1), pp. 77–87.

[20]. C. W. Wang (2007), "Nonlinear phenomena research perspectives", Nova Science Publishers, Inc. ISBN: 1-60021-520-3.

[21]. J. P. Eckmann, S. O. Kamphorst, D. Ruelle (1987), "Recurrence plots of dynamical systems", Europhysics Letters, vol. **5** (9), pp. 973–977.

[22]. A. J. Webster, R. O. Dendy and JET EFDA contributors (2013), "Statistical Characterisation and Classification of Edge Localised Plasma Instabilities", Physical Review Letters, vol. **110** (15), 155004.

[23]. W. H. Kruskal, W. A. Wallis (1952), "Use of ranks in one-criterion variance analysis", Journal of the American Statistical Association, vol. **47** (260), pp. 583–621.

[24]. J. Theiler, S. Eubank, A. Longtin, B. Galdrikian, J. D. Farmer (1992), "Testing for nonlinearity in time series: the method of surrogate data", Physica D: Nonlinear Phenomena, vol. **58** (1-4), pp. 77–94.

[25]. T. Schreiber, A. Schmitz (1996), "Improved surrogate data for nonlinearity tests", Physical Review Letters, vol. **77** (4), pp. 635–638.

[26]. A. Fraser, H. Swinney (1986), "Independent coordinates for strange attractors from mutual information", Physical Review A: Atomic, Molecular, and Optical Physics, vol. **33** (2), pp. 1134–1140.

[27]. F. Takens (1981), "Detecting strange attractors in turbulence". In D. A. Rand and L.-S. Young, "Dynamical Systems and Turbulence, Lecture Notes in Mathematics", Springer–Verlag, vol. 898, pp. 366–381.

[28]. J. Theiler (1990), "Estimating fractal dimension", Journal of the Optical Society of America A, vol. **7** (6), pp. 1055–1073.

[29]. M. B. Kennel, R. Brown, H. D. I. Abarbanel (1992), "Determining embedding dimension for phase-space reconstruction using a geometrical construction", Physical Review A, vol. **45** (6), pp. 3403–3411.

[30]. A. Galka (2000), "Topics in Nonlinear Time Series Analysis: With Implications for EEG", Advanced Series in Nonlinear Dynamics, World Scientific, Vol. 14.

[31]. T. Sauer (1995), "Interspike interval embedding of chaotic signals", Chaos: An Interdisciplinary Journal of Nonlinear Science, vol. **5** (1), pp. 127–132.

[32]. P. Grassberger, I. Procaccia (1983), "Measuring the strangeness of strange attractors", Physica D: Nonlinear Phenomena, vol. **9** (1–2), pp. 189–208.

[33]. A. Wolf, J. B. Swift, H. L. Swinney, J. A. Vastano, "Determining Lyapunov exponents from a time series, Physica D: Nonlinear Phenomena, vol. **16** (3), pp. 285–317.

[34]. M. Sano, Y. Sawada (1985), "Measurement of the Lyapunov spectrum from a chaotic time series", Physical Review Letters, vol. **55** (10), pp. 1082–1085.

[35]. H. Kantz, S. Schreiber (2004), "Nonlinear Time Series Analysis", Cambridge University Press, Cambridge University Press, UK. ISBN: 0-521-52902-6.

[36]. M. T. Rosenstein, J. J. Collins, C. J. De Luca (1993), "A practical method for calculating largest Lyapunov exponents from small data sets", Physica D: Nonlinear Phenomena, vol. **65** (1–2), pp. 117–134.

[37]. R. Hegger, H. Kantz, T. Schreiber (1999), "Practical implementation of nonlinear time series methods: The TISEAN package", Chaos: An Interdisciplinary Journal of Nonlinear Science, vol. **9** (2), pp. 413–435.

[38]. J. Iwanski, E. Bradley (1998), "Recurrence plots of experimental data: to embed or not to embed?", Chaos: An Interdisciplinary Journal of Nonlinear Science, vol. **8** (4), pp. 861–871.

[39]. D. Ruelle (1990), "Deterministic chaos: the science and the fiction", Proceedings of the Royal Society of London. Series A, Mathematical and Physical Sciences, vol. **427** (1873), pp. 241–248.

[40]. L. F. P. Franca, M. A. Savi (2003), "Evaluating noise sensitivity on the time series determination of Lyapunov exponents applied to the nonlinear pendulum", Shock and Vibration, vol. **10** (1), pp. 37–50.

[41]. J. B. Dingwell (2006), "Lyapunov Exponents", Wiley Encyclopedia of Biomedical Engineering.

[42]. C. Tsallis, A. R. Plastino, W. –M. Zheng (1997), "Power-law sensitivity to initial conditions – New entropic representation", Chaos, Solitons and Fractals, vol. **8** (6), pp. 885-891.

[43]. R. Klages (2013), "Weak chaos, infinite ergodic theory, and anomalous dynamics", book chapter in X. Leoncini and M. Leonetti, "From Hamiltonian Chaos to Complex Systems", Springer, Berlin, pp. 3–42. ISBN 978-1-4614-6961-2.

[44]. C. R. da Silva, H. R. da Cruz, M. L. Lyra (1999), "Low-dimensional non-linear dynamical systems and generalized entropy", Brazilian Journal of Physics, vol.**29** (1), pp. 144–152.

[45]. J. Gao, W. –W. Tung, Y. Cao, J. Hu, Y. Qi (2005), "Power-law sensitivity to initial conditions in a time series with applications to epileptic seizure detection", Physica A: Statistical Mechanics and its Applications, vol. **353**, pp. 613–624.

[46]. I. T. Jolliffe (2012), "Principal Component Analysis", Springer. ISBN: 0-387-95442-2.

[47]. D. S. Broomhead, G. P. King (1986), "Extracting Qualitative Dynamics from Experimental Data", Physica D: Nonlinear Phenomena, vol. **20** (2–3), pp. 217–236.

[48]. J. F. Gibson, J. D. Farmer, M. Casdagli, S. Eubank (1992), "An analytic approach to practical state space reconstruction", Physica D: Nonlinear Phenomena, vol. **57** (1–2), pp. 1–30.

[49]. G. P. King, R. Jones, D. S. Broomhead (1987), "Phase portraits from a time series: A singular system approach", Nuclear Physics B – Proceeding Supplements, vol. **2**, pp. 379–390.

[50]. E. J. Kostelich (1993), "Noise reduction in chaotic time–series data: a survey of common methods", Physical Review E: Statistical, Nonlinear and Soft Matters Physiscs, vol. **48** (3), pp. 1752–1763.

[51]. I. Michieli, B. Vojnović (2003), "Detecting noise in chaotic signals through principal component matrix transformation", Journal of Computing and Information Technology, vol.

11 (1), pp. 55–66.

[52]. K. Klimaszewska, J. J. Zebrowski (2009), "Detection of the type of intermittency using characteristic patterns in recurrence plots", Physical Review E: Statistical, Nonlinear and Soft Matter Physics, vol. **80**, p. 026214.

	Pulse Numbers	# of samples	Inputs	K-W Test (5%)
1	73397,73445,73446,73447,73450	246	2.5MA,2.4T,12.5-14.5MW,0.23-0.27	ungroupable
2	73484	108	2.5MA,2.4T,14.8MW,0.28	/
3	74130	78	2.5MA,2.4T,13.6MW,0.25	/
4	74364	116	2MA,1.8T,15.5MW,0.36	/
5	74365,74366,74367,74368,74369,74371, 74372,74373,74374,74375	347	2.5MA,2.5T,15.5-18.5MW,0.34-0.35	ungroupable
6	74375,74376	54	2.5MA,2.5T,15.1-15.5MW,0.33-0.35	groupable
7	74378,75724,75726,75727,75728,75731, 75732,76481	497	2MA,2T,11-12.8MW,0.32-0.37	ungroupable
8	74378,75724,75726,75727,75728,75731, 75732,76476	497	2MA,2T,12.1-14.5MW,0.32-0.37	ungroupable
9	74378,75724,75728,75731,75732,76473, 76474,76475,76476,76477,76478,76479	705	2MA,2T,12.5-15.2MW,0.32-0.37	ungroupable
10	74443,74444	90	2.5MA,2.7T,14-15.8MW,0.32	groupable
11	74612,74613,77073	291	2.6MA,2.3-2.4T,16.7-17MW,0.36	ungroupable
12	74793,74795	286	1.7MA,1.6T,9.1-10.5MW,0.35-0.36	ungroupable
13	74798	120	1.7MA,1.6T,16.8MW,0.37	/
14	75118	33	1.7MA,1.8T,9.4MW,0.26	/
15	75724,75728,76471,76472,76473,76474, 76475,76476,76477,76478,76479	439	2MA,2T,12.6-15.4MW,0.32-0.37	ungroupable
16	76428,76430,76431,76437,76438	197	2MA,2T,7.5MW,0.35	groupable
17	76440,76443,77192	126	2MA,2T,7.5-8.4MW,0.31-0.36	ungroupable
18	76470,76480	45	2MA,2T,16.8-19.8MW,0.37	ungroupable
19	76470,76471,76472,76473,76474,76475, 76476,76477,76478,76479	363	2MA,2T,14.5-16.8MW,0.35-0.37	groupable
20	76812	60	2MA,1.8T,18.5MW,0.37	/
21	78448	19	2.5MA,2.7T,12.9MW,0.4	/
22	78750	104	1.5MA,1.8T,17.6MW,0.32	/
23	79389	132	2MA,2T,11.9MW,0.32	/
24	79546	177	1.5MA,1.8T,17.7MW,0.45	/

Table I: Groups with division by input conditions (plasma current, toroidal magnetic field, NBI input power and lower triangularity) and belonging to the same experiment.

Pulse No:	*m*	Pulse No:	*m*
74375	5	76471	5
74376	5	76472	5
74443	4	76473	5
74444	5	76474	5
76428	7	76475	6
76430	6	76476	5
76431	6	76477	5
76437	7	76478	6
76438	6	76479	5
76470	5	–	–

Table II. Values of m for Dα time series.

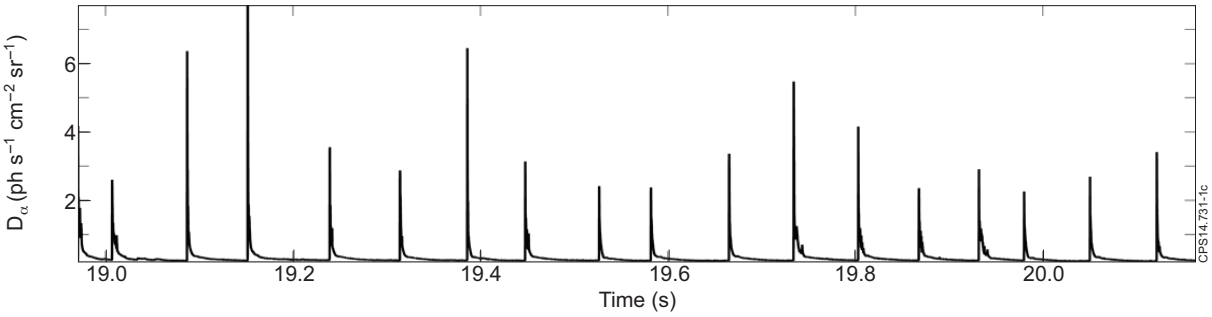

Figure 1: Dα time series for Pulse No: 74375.

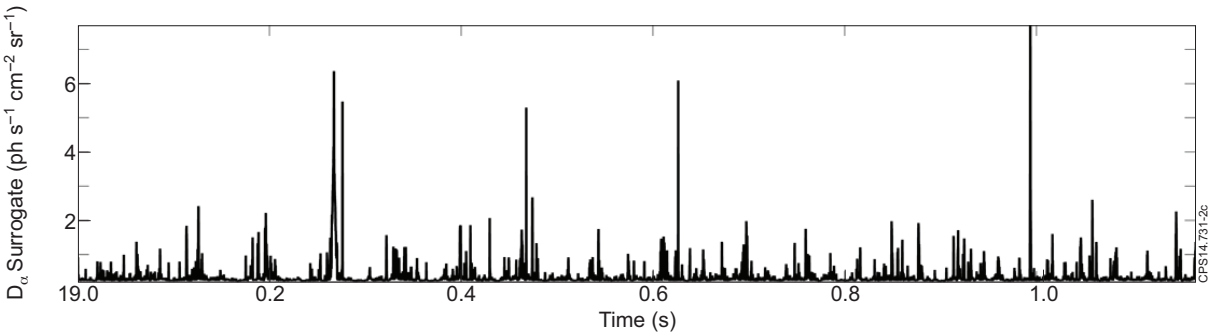

Figure 2: Surrogate time series for Pulse No: 74375.

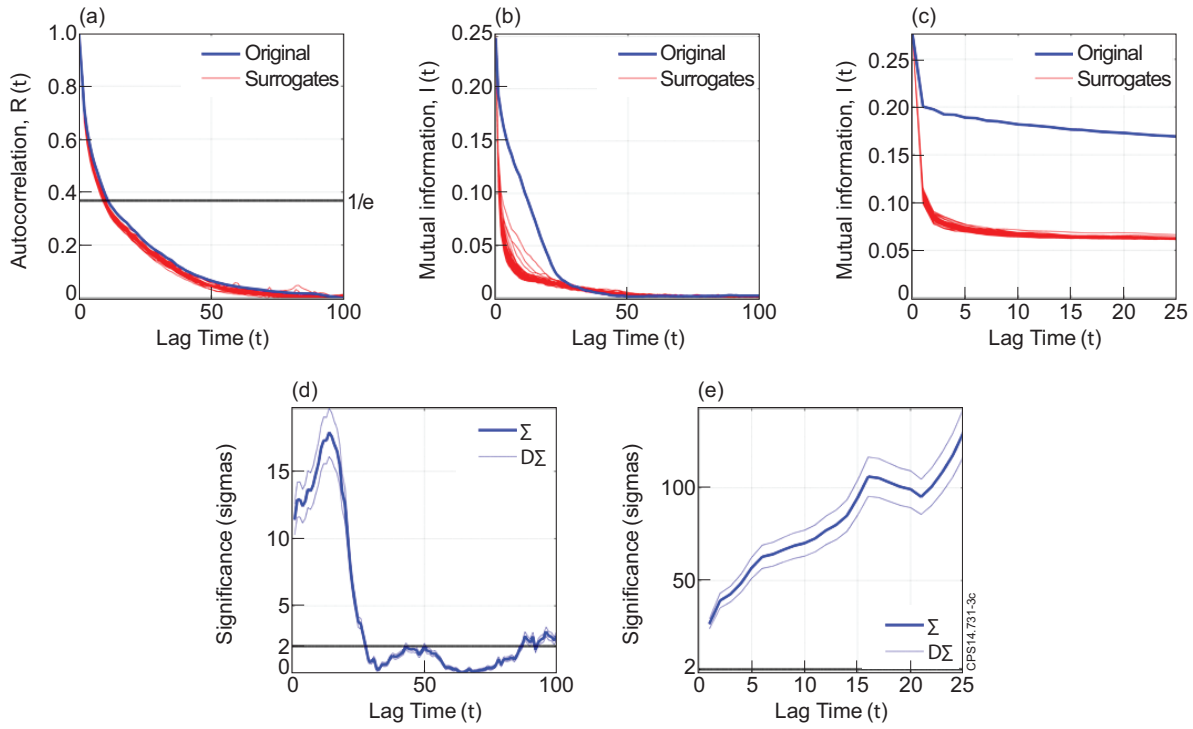

Figure 3: Autocorrelation function (a) and TDMI of the Dα time series and its surrogate for Pulse No: 74375 with (b) equal size bins and (c) equal probability bins; significance of the TDMI with (d) equal size bins and (e) equal probability bins, with error bar.

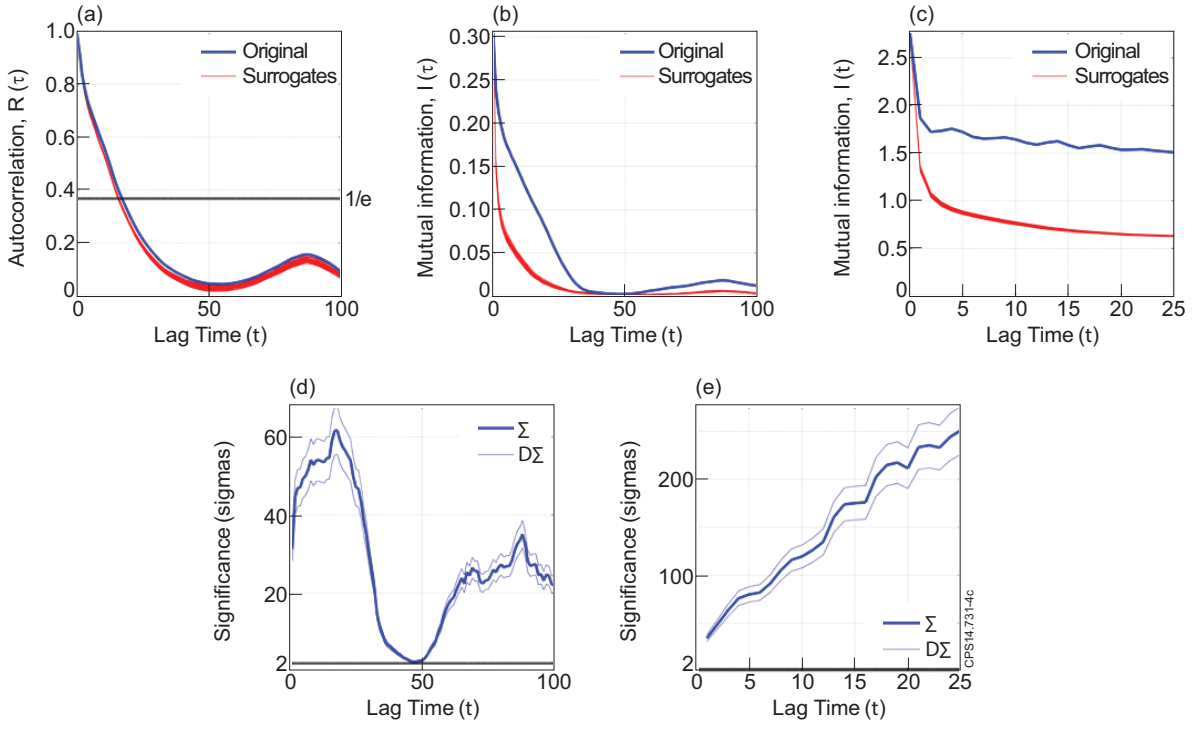

Figure 4: Autocorrelation function (a) and TDMI of the Dα time series and its surrogate for Pulse No: 76428 with (b) equal size bins and (c) equal probability bins; significance of the TDMI with (d) equal size bins and (e) equal probability bins with error bar.

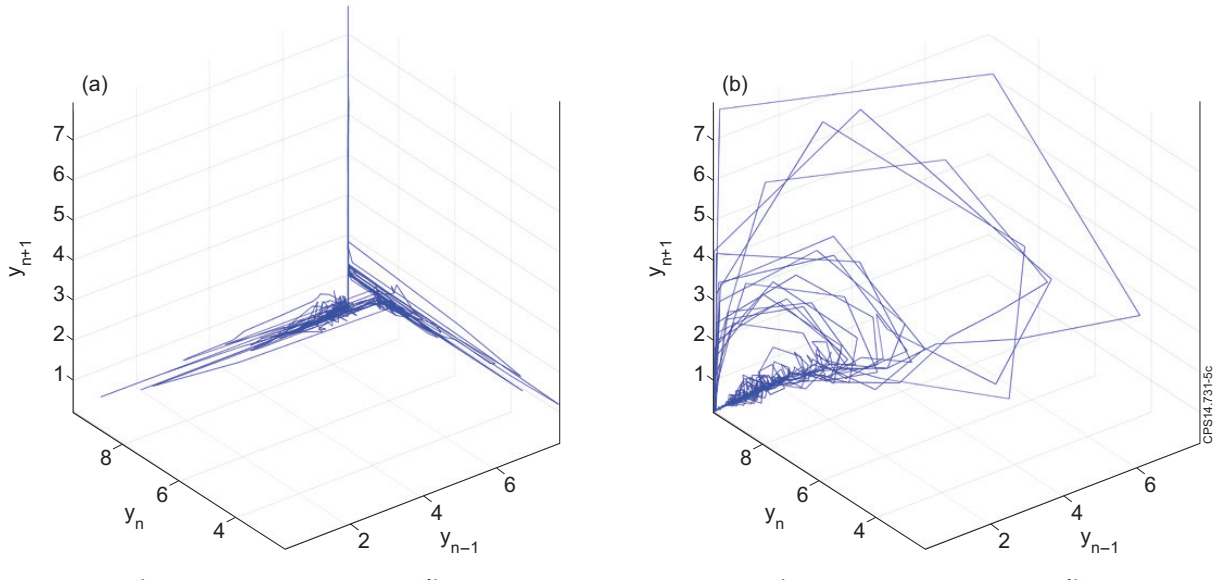

Figure 5: 3D Projection for different time delay reconstructions: a) $\tau^* = 11$, b) $\tau^* = 1$.

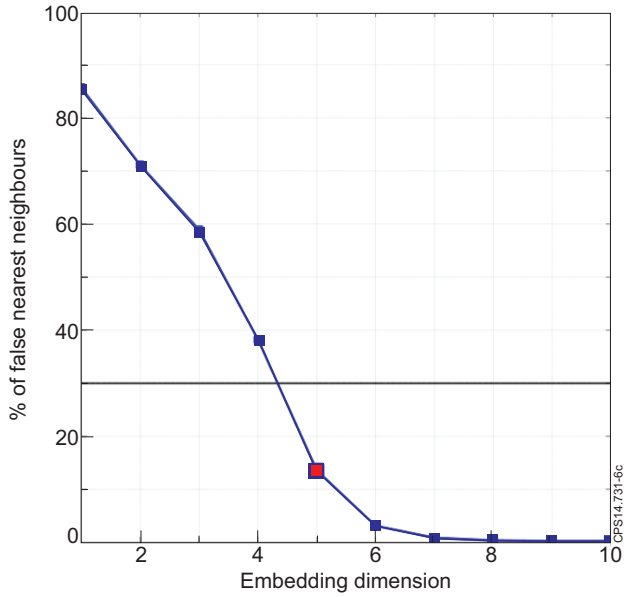

Figure 6: Percentage of false nearest neighbours for Pulse No: 74375, using $\tau^* = 1$.

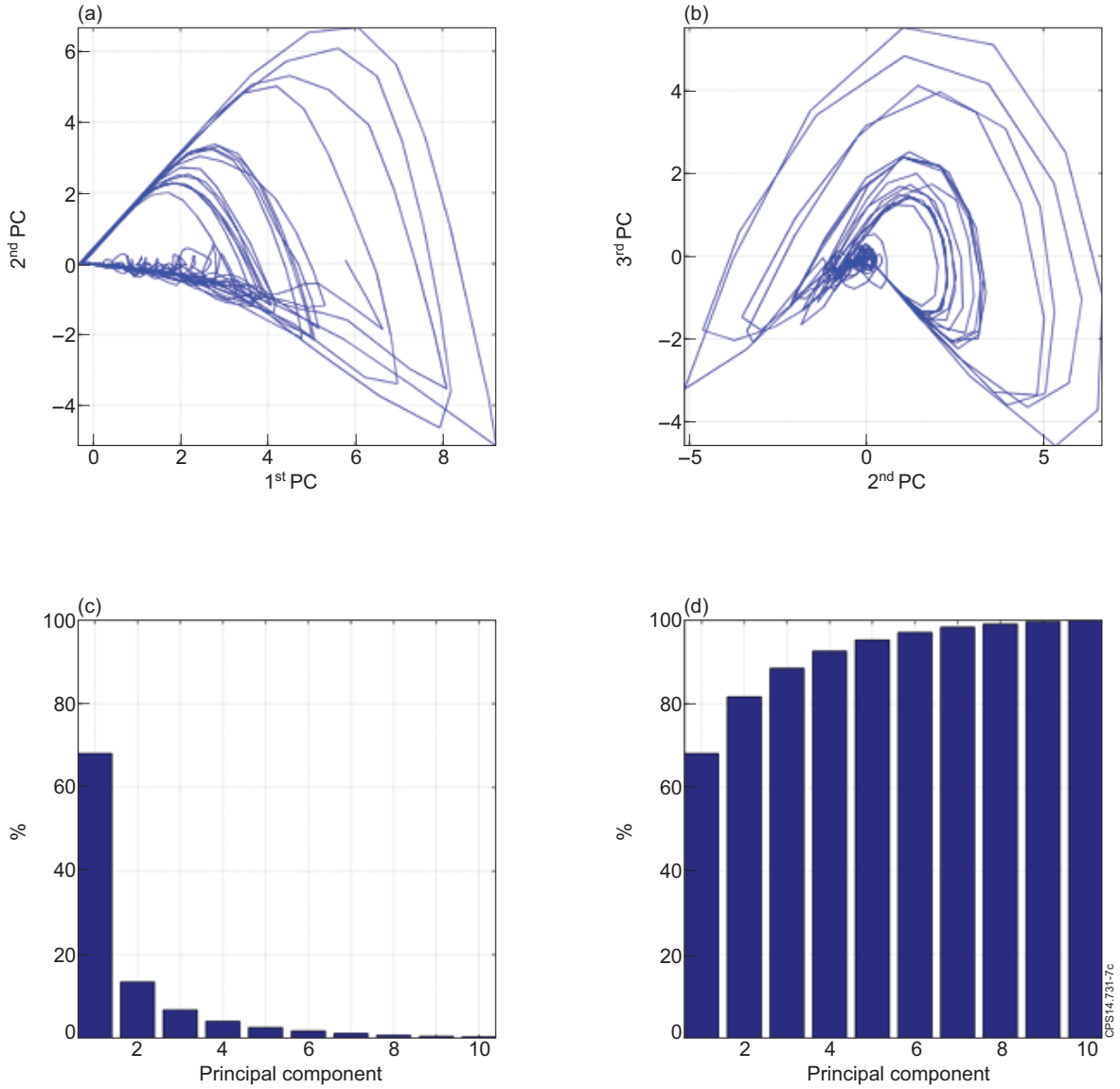

Figure 7: Projections of the embedding space on the plane described: a) by the first and second PCs; b) by the second and third PCs; c) percentage of variance described by each PC; d) cumulative percentage of variance described by the PCs

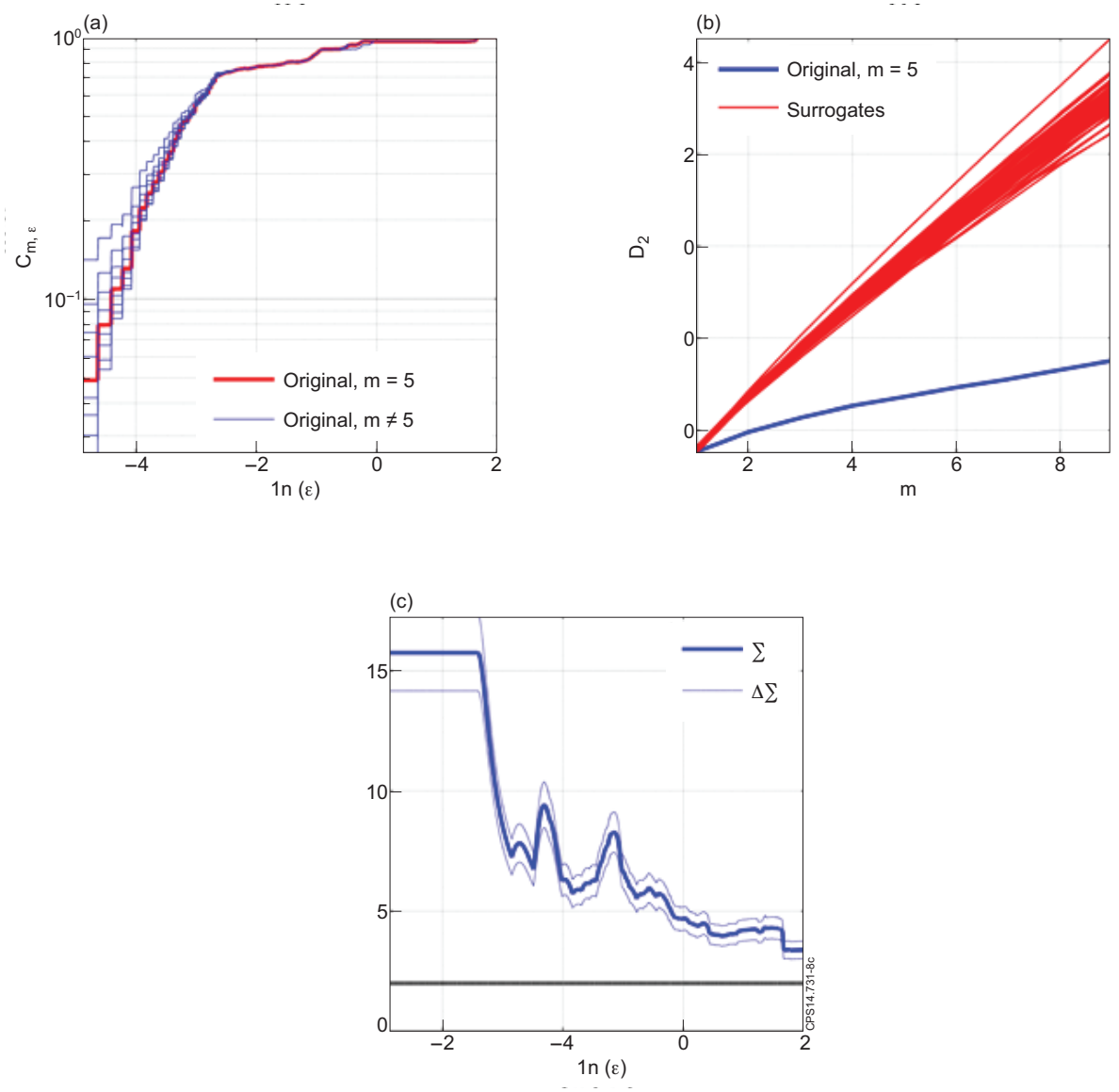

Figure 8 (a) Correlation integral $C_{m,\varepsilon}$ as a function of ln(ε) for different values of m, (b) correlation dimension D2 as a function of m for the original time series and surrogates and (c) significance of the correlation dimension with error bar with m = 5, for Pulse No: 74375.

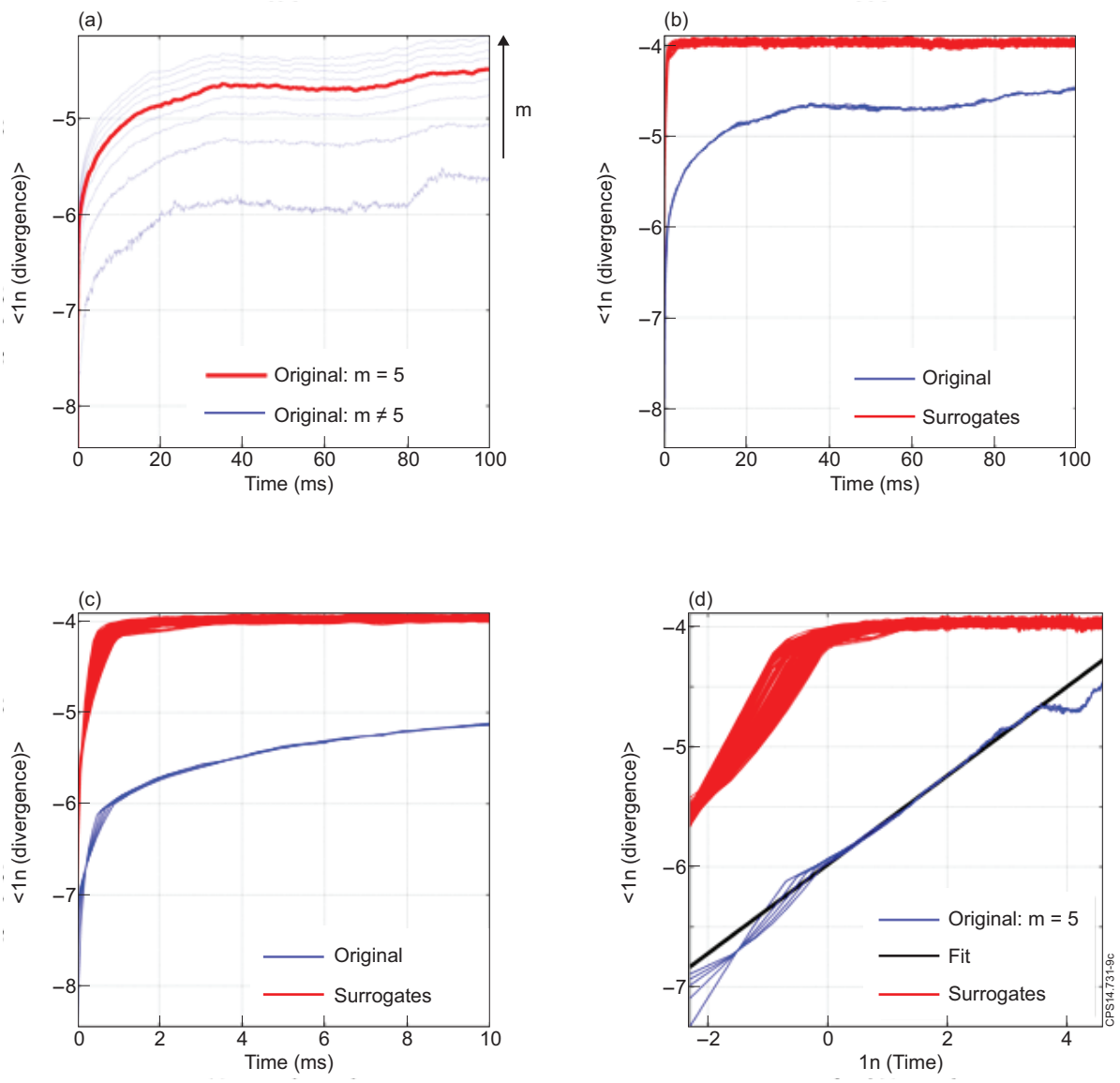

Figure 9: a) Mean logarithm of divergence for Pulse No: 74375 for the original time series for different values of m; b) c) different zooms of the translated version of the mean logarithm of divergence for Pulse No: 74375 for the original time series and surrogates; d) translated version of the mean logarithm of divergence in semi-logarithmic scale for Pulse No: 74375 for the original time series, its fitting and surrogates.

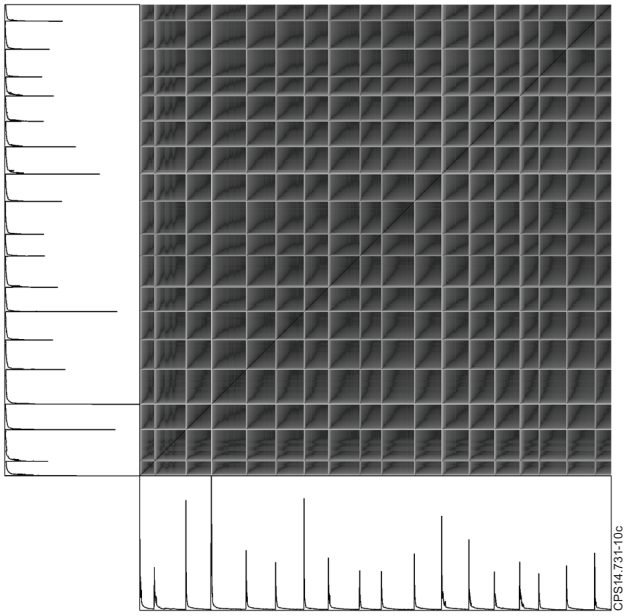

Figure 10: UTRP for Pulse No: 74375.

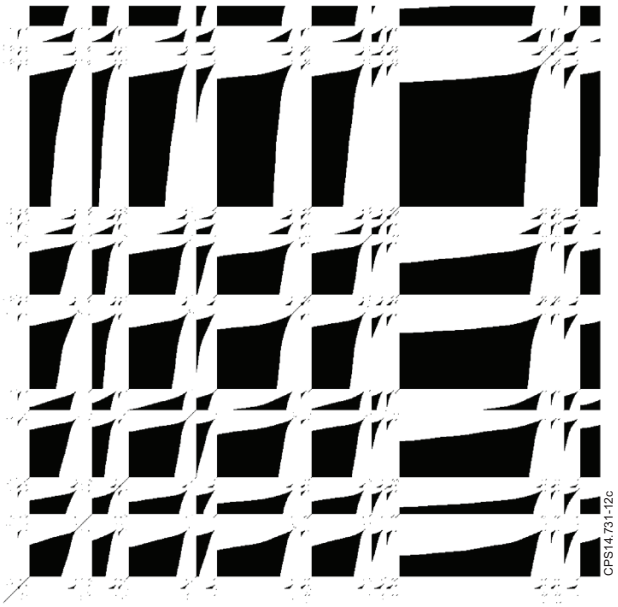

Figure 12: RP for type-II intermittency.

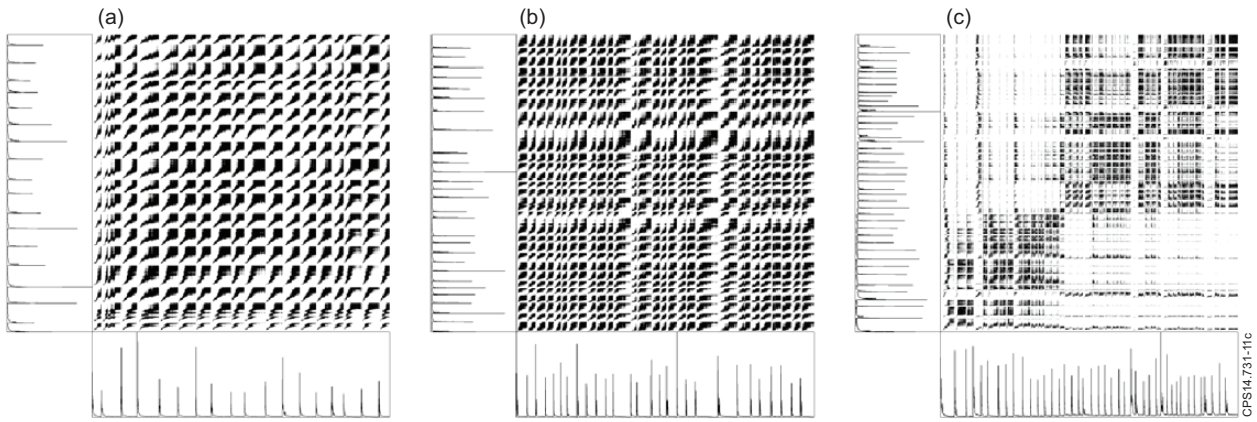

Figure 11: RP for Pulse No's: (a) 74375 (b) 76430 (c) 74444.